

# High Chromium White Irons



# High Chromium White Irons:

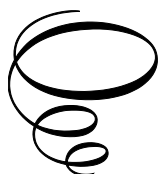
*Properties and Wear Resistance*

By

Dipak Kumar Mondal

and Siddhartha Sankar Mandal

**Cambridge  
Scholars  
Publishing**



High Chromium White Irons: Properties and Wear Resistance

By Dipak Kumar Mondal and Siddhartha Sankar Mandal

This book first published 2026

Cambridge Scholars Publishing

Lady Stephenson Library, Newcastle upon Tyne, NE6 2PA, UK

British Library Cataloguing in Publication Data

A catalogue record for this book is available from the British Library

Copyright © 2026 by Dipak Kumar Mondal and Siddhartha Sankar Mandal

All rights for this book reserved. No part of this book may be reproduced, stored in a retrieval system, or transmitted, in any form or by any means, electronic, mechanical, photocopying, recording or otherwise, without the prior permission of the copyright owner.

ISBN: 978-1-0364-6898-9

ISBN (Ebook): 978-1-0364-6899-6

Dedicated to  
Scholars and Institutions  
Engaged in Academic and Industry Research



# TABLE OF CONTENTS

List of Figures.....	xi
List of Tables.....	xvi
Preface.....	xviii
Introduction.....	xx
Chapter 1.....	1 - 29
Published Works on Chromium White Irons Dipak Kumar Mondal & Siddhartha Sankar Mandal	
1.1 As-cast High Chromium White Cast Iron	
1.1.1 Composition	
1.1.2 Solidification Behaviour and Microstructure	
1.1.3 Eutectic Structure	
1.1.4 Formation of $M_7C_3$ Carbides	
1.2 Control of Matrix Microstructure	
1.2.1 Destabilization heat treatment	
1.2.2 Precipitation of Secondary Carbides during Destabilization Treatment	
1.2.3 Transformation of a destabilized matrix	
1.2.4 Post-destabilization Heat Treatment	
1.3 Abrasive Wear Performance of High Chromium White Irons	
1.3.1 Types of Abrasive Wear	
1.3.2 Mechanism of Wear	
1.4 Influence of Microstructure on Wear Performance	
1.4.1 Effect of Eutectic Carbides on Abrasive Wear Performance	
1.4.2 Effect of Matrix Microstructure on Abrasive Wear Performance	
1.5 Effect of Abrasive Features on Wear Performance	
1.6 Effect of Alloy Composition on Wear Performance	
1.7 Fracture Toughness of High Chromium White Irons	
1.8 Repeated Impact Resistance of Chromium White Irons	
1.9 Electrochemical Corrosion Behaviour of High Chromium White Irons	
1.10 References	

Chapter 2 .....	30 - 48
As-cast Microstructure, Hardness and Wear Studies of 8.0%, 16.0% and 20.0% (by wt.) Chromium White Irons	
Dipak Kumar Mondal & Siddhartha Sankar Mandal	
2.1	Introduction
2.2	Alloy Preparation and Chemical Analysis
2.3	Microstructure
2.3.1	As-cast Microstructure of Alloy-1
2.3.2	As-cast Microstructure of Alloy-2
2.3.3	As-cast Microstructure of Alloy-3
2.4	As-cast Alloy Hardness
2.5	As-cast Wear Performance
2.5.1	Surface Observation
2.5.2	Cumulative Wear Loss
2.6	Conclusions
2.7	References
 Chapter 3 .....	 49 - 52
Destabilization Heat Treatment and Associated Test Techniques	
Dipak Kumar Mondal & Siddhartha Sankar Mandal	
3.1	Introduction
3.2	Steps of Conducting Continuous Destabilization and Cyclic Destabilization
3.3	Optical microscopy, Electron Microscopy and XRD Analysis
3.4	Hardness Measurement and Impact Testing
3.5	Wear Test
3.6	References
 Chapter 4 .....	 53 - 74
Continuous Destabilization versus Cyclic Destabilization of As-Cast Alloy-1	
Dipak Kumar Mondal & Siddhartha Sankar Mandal	
4.1	Introduction
4.2	Microstructure
4.3	Hardness
4.4	Impact toughness
4.5	Wear After Continuous Destabilization of Alloy-1
4.5.1	Surface Observation
4.5.2	Cumulative Wear
4.6	Wear After Cyclic Destabilization of Alloy-1
4.6.1	Surface Observation

4.6.2 Cumulative Wear	
4.7 Conclusions	
4.8 References	
Chapter 5 .....	75 - 91
Continuous Destabilization versus Cyclic Destabilization of As-Cast Alloy-2	
Dipak Kumar Mondal & Siddhartha Sankar Mandal	
5.1 Introduction	
5.2 Microstructure	
5.3 Hardness	
5.4 Impact toughness	
5.5 Wear After Continuous Destabilization of Alloy-2	
5.5.1 Surface Observation	
5.5.2 Cumulative Wear	
5.6 Wear After Cyclic Destabilization of Alloy-2	
5.6.1 Surface Observation	
5.6.2 Cumulative Wear	
5.7 Conclusions	
5.8 References	
Chapter 6 .....	92 - 111
Continuous Destabilization versus Cyclic Destabilization of As-Cast Alloy-3	
Dipak Kumar Mondal & Siddhartha Sankar Mandal	
6.1 Introduction	
6.2 Microstructure	
6.3 Hardness	
6.4 Impact toughness	
6.5 Wear After Continuous Destabilization of Alloy-3	
6.5.1 Surface Observation	
6.5.2 Cumulative Wear	
6.6 Wear After Cyclic Destabilization of Alloy-3	
6.6.1 Surface Observation	
6.6.2 Cumulative Wear	
6.7 Conclusions	
6.8 References	

Chapter 7 .....	112 - 127
Electrochemical Behaviour of As-cast and Destabilized Alloys-1, 2 and 3	
Dipak Kumar Mondal & Siddhartha Sankar Mandal	
7.1 Introduction	
7.2 Steps of Electrochemical Measurements	
7.3 Electrochemical Behaviour of As-cast Alloys	
7.4 Electrochemical Behaviour of Destabilized Alloys	
7.4.1 Destabilized Alloy-1(A1)	
7.4.2 Destabilized Alloy-2(A2)	
7.4.3 Destabilized Alloy-3(A3)	
7.5 Conclusions	
7.6 References	
Chapter 8 .....	128 - 130
Summarized Highlights	
Dipak Kumar Mondal & Siddhartha Sankar Mandal	
Chapter 9 .....	131 - 134
General Discussion and Scopes for Further Studies	
Dipak Kumar Mondal & Siddhartha Sankar Mandal	
9.1 General discussion	
9.2 Scopes for further studies	

## LIST OF FIGURES

1.1	Iron-chromium-carbon liquidus surface showing the composition range of commonly used hypoeutectic white irons.
1.2	SEM showing hexagonal shell (arrow) of $M_7C_3$ carbide in dark matrix of austenite (5000X).
1.3	Steps illustrating formation of austenite (A) and hexagonal morphology of $M_7C_3$ carbides.
1.4	A rosette structure accommodating $M_7C_3$ (arrow) carbide network (750X).
1.5	Destabilization temperature versus hardness and retained austenite content.
1.6	Idealised view of an abrasive wear groove.
1.7	Situations representing large and small ratio of abrasive grit size to matrix mean-free path.
1.8	Specimen geometries used in fracture toughness tests of chromium white irons.
1.9	Stress patterns developed in plastic and rigid matrix at the Point of impact by a falling ball.
2.1	Optical micrographs of as-cast alloy-1 showing dendrites of pearlite plus martensite along with: (a) netted eutectic carbides, and (b) discontinuous pattern of rods and plate shaped eutectic carbides.
2.2	XRD pattern of as-cast alloy-1.
2.3	Scanning electron micrograph (SEM) of alloy-1 (2000X).
2.4	EDS analysis in a carbide cluster of as-cast alloy-1.
2.5	Optical micrographs of as-cast alloy-2 revealing escalated eutectic regions with (a) clusters of rods, fibres and discontinuous carbides, and (b) a region containing refined eutectic carbides.
2.6	XRD pattern of as-cast alloy-2.
2.7	Scanning electron micrograph (SEM) of alloy-2 (5000X).
2.8	Optical micrographs of alloy-3 showing (a) eutectic structure, and (b) clustering of eutectic carbides.
2.9	XRD pattern of as-cast alloy-3.
2.10	Scanning electron micrograph (SEM) of alloy-3 (2000X).

2.11	Effect of chromium content on bulk hardness and matrix hardness.
2.12	SEM images of worn-out surfaces of alloy-1 abraded under (a) 19.6N load, and (b) 49.0N load.
2.13	SEM images of worn-out surfaces of alloy-2 abraded under (a) 19.6N load, and (b, c, d) 49.0N load.
2.14	SEM images of alloy-2 wear debris consisting of long chips shaped (a) straight and (b) wrinkled.
2.15	SEM images of worn-out surfaces of alloy-3 abraded under (a) 19.6N and (b) 49.0N loads, and (c) wear debris produced by delamination of oxide layer.
2.16	Abrasive wear graphs of alloys-1, 2 and 3, and also of Ni-hard IV derived under (a) 19.6N load and (b) 49.0N load.
4.1	Optical micrographs (a, b, c) and scanning electron micrographs (d, e, f) of alloy-1 subjected to continuous destabilization at (a, d) 900°C, (b, e) 1000°C, and (c, f) 1100°C.
4.2	XRD profiles of alloy-1 after continuous destabilization at (a) 900°C, (b) 1000°C, and (c) 1100°C.
4.3	Optical micrographs (a, b, c) and scanning electron micrographs (d, e, f) of alloy-1 subjected to cyclic destabilization at (a, d) 900°C, (b, e) 1000°C, and (c, f) 1100°C.
4.4	XRD profiles of alloy-1 after cyclic destabilization at (a) 900°C, (b) 1000°C, and (c) 1100°C.
4.5	Impact fracture surfaces of alloy-1 subjected to continuous destabilization (a, b and c) and cyclic destabilization (d, e and f) at 900°C (a, d), 1000°C (b, e) and 1100°C (c, f).
4.6	Wear surfaces and debris of alloy-1 subjected to continuous destabilization at (a) 900°C, (b) 1000°C, and (c, d) 1100°C, and abraded under 19.6N load.
4.7	Wear surfaces and debris of alloy-1 subjected to continuous destabilization at (a, d) 900°C, (b, e) 1000°C, and (c, f) 1100°C and abraded under 49.0N load.
4.8	Cumulative wear versus sliding distance plots of alloy-1 subjected to continuous destabilization, and tested under (a) 19.6N load and (b) 49.0N load.
4.9	Wear surfaces and wear debris formed under 19.6N load for alloy-1 subjected to cyclic destabilization at (a, d, e) 900°C, (b) 1000°C, and (c, f) 1100°C.

4.10	Wear surfaces and wear debris formed under 49.0N load for alloy-1 subjected to cyclic destabilization at (a, d) 900°C, (b) 1000°C, and (c, e) 1100°C.
4.11	Cumulative wear versus sliding distance plots of alloy-1 subjected to cyclic destabilization and tested under (a) 19.6N load and (b) 49.0N load.
5.1	Optical micrographs (a, b, c) and scanning electron micrographs (d, e, f) of alloy-2 subjected to continuous destabilization at (a, d) 900°C, (b, e) 1000°C, and (c, f) 1100°C.
5.2	XRD patterns of alloy-2 subjected to continuous destabilization at a) 900°C, b) 1000°C, and c) 1100°C.
5.3	Optical micrographs (a, b, c) and scanning electron micrographs (d, e, f) of alloy-2 subjected to cyclic destabilization at (a, d) 900°C, (b, e) 1000°C, and (c, f) 1100°C.
5.4	XRD patterns of alloy-2 subjected to cyclic destabilization at a) 900°C, b) 1000°C, and c) 1100°C.
5.5	Impact fracture surfaces of alloy-2 subjected to continuous destabilization (a, b and c) and cyclic destabilization (d, e and f) at 900°C (a, d), 1000°C (b, e) and 1100°C (c, f).
5.6	Wear surfaces and wear debris formed under 19.6N wear load for alloy-2 subjected to continuous destabilization at (a) 900°C, (b) 1000°C, and (c, d) 1100°C.
5.7	Wear surfaces and wear debris formed under 49.0N wear load for alloy-2 subjected to continuous destabilization at (a) 900°C, (b) 1000°C, and (c, d) 1100°C.
5.8	Cumulative wear versus sliding distance plots of alloy-2 subjected to continuous destabilization and tested under (a) 19.6N load and (b) 49.0N load.
5.9	Wear surfaces of alloy 2 subjected to cyclic destabilization at (a, d) 900°C, (b, e, f) 1000°C and (c) 1100°C, and tested at (a, b, c) 19.6N load and (d, e, f) 49.0N load.
5.10	Wear debris formed under (a, b) 19.6N load and (c, d) 49.0N load for alloy-2 subjected to cyclic destabilization at (a, b) 900°C and (c, d) 1000°C.
5.11	Cumulative wear versus sliding distance plots of alloy-2 subjected to cyclic destabilization and tested under (a) 19.6N load and (b) 49.0N load.

6.1	Optical micrographs ( <i>a, b, c</i> ) and scanning electron micrographs ( <i>d, e, f</i> ) of alloy-3 subjected to continuous destabilization at ( <i>a, d</i> ) 900°C, ( <i>b, e</i> ) 1000°C, and ( <i>c, f</i> ) 1100°C.
6.2	FESEM images of alloy-3 subjected to continuous destabilization at ( <i>a</i> ) 900°C and ( <i>b</i> ) 1100°C.
6.3	XRD patterns of alloy-3 subjected to continuous destabilization at ( <i>a</i> ) 900°C, ( <i>b</i> ) 1000°C, and ( <i>c</i> ) 1100°C.
6.4	Optical micrographs ( <i>a, b, c</i> ) and scanning electron micrographs ( <i>d, e, f</i> ) of alloy-3 subjected to cyclic destabilization at ( <i>a, d</i> ) 900°C, ( <i>b, e</i> ) 1000°C, and ( <i>c, f</i> ) 1100°C.
6.5	FESEM images of alloy-3 subjected to cyclic destabilization at ( <i>a</i> ) 1000°C and ( <i>b</i> ) 1100°C.
6.6	XRD patterns of alloy-3 after cyclic destabilization at ( <i>a</i> ) 900°C, ( <i>b</i> ) 1000°C, and ( <i>c</i> ) 1100°C.
6.7	Impact fracture surfaces of alloy-3 subjected to: ( <i>a, b, c</i> ) continuous destabilization and ( <i>d, e, f</i> ) cyclic destabilization at ( <i>a, d</i> ) 900°C, ( <i>b, e</i> ) 1000°C and ( <i>c, f</i> ) 1100°C.
6.8	Wear surfaces and debris formed under 19.6N load for alloy-3 subjected to continuous destabilization at ( <i>a, d</i> ) 900°C, ( <i>b, c, e</i> ) 1000°C, and ( <i>f</i> ) 1100°C.
6.9	Wear surfaces and wear debris formed under 49.0N load for alloy-3 subjected to continuous destabilization at ( <i>a</i> ) 900°C, ( <i>b, d</i> ) 1000°C, and ( <i>c</i> ) 1100°C.
6.10	Cumulative wear versus sliding distance plots of alloy-3 subjected to continuous destabilization and tested under ( <i>a</i> ) 19.6N load and ( <i>b</i> ) 49.0N load.
6.11	Wear surfaces and wear debris formed under 19.6N load for alloy-3 subjected to cyclic destabilization at ( <i>a, d</i> ) 900°C, ( <i>b, e</i> ) 1000°C, and ( <i>c</i> ) 1100°C.
6.12	Wear surfaces and wear debris formed under 49.0N load for alloy-3 subjected to cyclic destabilization at ( <i>a</i> ) 900°C, ( <i>b, d</i> ) 1000°C, and ( <i>c, e</i> ) 1100°C.
6.13	Cumulative wear versus sliding distance plots of alloy-3 subjected to cyclic destabilization and tested under ( <i>a</i> ) 19.6N load and ( <i>b</i> ) 49.0N load.
7.1	Schematic representation of electrochemical cell with computer-controlled potentiostat / galvanostat.

7.2	Polarization curves of as-cast alloys-1, 2 and 3 at (a) pH7 solution, (b) pH2 solution, and (c) pH12 solution of 1.0 wt.% NaCl.
7.3	Corroded surfaces of as-cast alloy-1 at pH7 and pH12 (a, b), alloy-2 at pH7 (c), and alloy-3 at pH12 (d).
7.4	Potentiodynamic polarization curves with 1.0 wt.% NaCl solution at pH 7 (a, b), pH2 (c, d) and pH 12 (e, f) for alloy-1(A1) subjected to continuous destabilization (a, c, e) and cyclic destabilization (b, d, f) at different temperatures.
7.5	Potentiodynamic polarization curves with 1.0 wt.% NaCl solution at pH7 (a, b), pH 2 (c, d) and pH 12 (e, f) for alloy-2(A2) subjected to continuous destabilization (a, c, e) and cyclic destabilization (b, d, f) at different temperatures.
7.6	Potentiodynamic polarization curves with 1.0 wt.% NaCl solution at pH7 (a, b), pH 2 (c, d) and pH 12 (e, f) for alloy-3(A3) subjected to continuous (a, c, e) and cyclic (b, d, f) destabilization at different temperatures.

## LIST OF TABLES

1.1	Chemical compositions of some common white iron alloys
1.2	Hardness of abrasive materials relative to hardness of micro-constituents that occur in alloy white irons.
2.1	Proposed composition ranges of the alloyed white irons.
2.2	Chemical composition of alloys- 1, 2, and 3 in wt.%.
2.3	List of $2\theta$ and corresponding $d$ -values for peaks of some matrix phases.
2.4	Percent carbide and matrix in as-cast microstructure.
2.5	Microhardness (VHN) data before and after wear.
4.1	Volume percent of eutectic and secondary carbides and average particle diameter ( $\mu m$ ) of secondary carbides in alloy-1, subjected to continuous and cyclic destabilization.
4.2	Hardness (HV) of alloy-1 in as-cast state and after continuous and cyclic destabilization.
4.3	Charpy notched impact values of alloy-1 in as-cast state, and after continuous and cyclic destabilization treatment.
4.4	Micro-hardness values of the worn-out surfaces of alloy-1 subjected to cyclic destabilization treatment.
5.1	Hardness (HV) of alloy-2 in as-cast state, and after continuous and cyclic destabilization treatment.
5.2	Charpy notched impact values of alloy-2 in as-cast state, and after continuous and cyclic destabilization treatment.
5.3	Micro-hardness after wear under 19.6N load and 49.0N load for alloy-2 subjected to cyclic destabilization.
6.1	Hardness (HV) of alloy-3 in as-cast state, and after continuous and cyclic destabilization treatment.
6.2	Notched Charpy impact values of alloy-3 in as-cast state, and after continuous and cyclic destabilization treatment.
6.3	Hardness before wear versus micro-hardness after wear under 19.6N load and 49.0N load for alloy-3 subjected to continuous destabilization.
6.4	Hardness before wear versus micro-hardness after wear under 19.6N load and 49.0N load for alloy-3 subjected to cyclic Destabilization.

7.1	Electrochemical data of as-cast alloys-1, 2 and 3 in 1.0 wt.% NaCl solution at different pH levels.
7.2	Electrochemical data of alloy-1(A1) in as-cast state and after continuous destabilization at different temperatures and tested in 1.0 wt.% NaCl solution with varying pH values.
7.3	Electrochemical data of alloy-1(A1) after cyclic destabilization at different temperatures and tested in 1.0 wt.% NaCl solution with varying pH values.
7.4	Electrochemical data of alloy-2(A2) after continuous destabilization at different temperatures and tested in 1.0 wt.% NaCl solution with varying pH values.
7.5	Electrochemical data of alloy-2(A2) after cyclic destabilization at different temperatures and tested in 1.0 wt.% NaCl solution with varying pH values.
7.6	Electrochemical data of alloy-3(A3) after continuous destabilization at different temperatures, and tested in 1.0 wt.% NaCl solution with varying pH values.
7.7	Electrochemical data of alloy-3(A3) after cyclic destabilization at different temperatures, and tested in 1.0 wt.% NaCl solution with varying pH values.

## PREFACE

This book provides experimental insight into improving wear resistance through microstructural optimization of high chromium white irons.

The importance of high chromium white irons has long been acknowledged; while their service performances have been recognized to be a function of microstructure, hardness, and associated abrasive wear resistance under impact. The proposed title also appears to explore the role of microstructure, hardness and impact toughness towards building wear resistance in a series of experimental chromium white irons, as-cast and destabilized.

It is important to mention that the contents of a PhD thesis, submitted by the second author and supervised by the first author, are duly edited and shaped in the form of a book. The book primarily focuses on preparing a series of chromium white irons with varying chromium contents and establishing the role of as-cast microstructure, hardness and impact toughness in deriving the as-cast wear resistance. Further, it incorporates a substantial discussion on two different routes of destabilization heat treatment, namely, the usually conducted continuous destabilization and the newly introduced cyclic destabilization. More precisely, this book upholds the unique role of cyclic destabilization towards refining the as-cast eutectic carbides and developing a matrix microstructure, capable of improving wear resistance of the experimental alloys to a significantly high level. Attempts are also made to study electrochemical behaviour of the as-cast and destabilized alloys in saline solutions with varying pH levels. All findings so obtained are expected to benefit the potential readers and researchers working in this area. Industries may also plan to implement the idea and thoughts adopted in this book to develop wear resistant chromium white irons.

The authors express gratitude for all kinds of support extended by the faculty and staff members of the Department of Metallurgical and Materials Engineering at NIT Durgapur, India during conduct of tests as well as experiments in different laboratories. Assistance from Dr K S Ghosh, Professor of this Department and Institute is acknowledged with thanks for guiding us and contributing ideas while writing on the electrochemical behaviour of the as-cast and destabilized alloys in Chapter 7. The authors

are also indebted to the scientists and technicians of the SEM laboratory in Central Mechanical Engineering Research Institute at Durgapur, India for providing support to undertake electron microscopy of samples, as and when needed.

Finally, the authors gratefully acknowledge the invaluable support provided by the first author's son, Mr. Abhro Jyoti Mondal, for shaping all the curves and diagrams in this book with meticulous attention and accurate labeling of various features.

# INTRODUCTION

High chromium white irons of hypoeutectic grade containing 11.0 – 30.0 wt.% chromium and 2.0 – 3.0 wt.% carbon along with nickel, molybdenum, manganese, silicon, and traces of sulphur, and phosphorous, are widely used in mining, grinding, and materials handling plants. In all cases, their performance during service is a function not only of the microstructure, strength and hardness, but also the abrasive wear resistance and ability to withstand impact. As-cast microstructure of high chromium white irons consists primarily of austenite dendrites and inter-dendritic eutectic of partially transformed austenite and  $M_7C_3$ , where 'M' represents the metallic species like iron and chromium. The majority of the chromium content in this alloy is combined with carbon to form carbide, thus leaving a chromium-depleted austenite on heating with poor hardenability. To regain the hardenability of the austenite, molybdenum, along with nickel and copper, is added to high chromium white irons in excess of 1.0% (by wt.). Eutectic carbides usually occur in the form of  $M_7C_3$  rods; while duplex carbides bearing  $M_7C_3$  encased with a layer of  $M_3C$  may also appear following solid-state diffusion during post-solidification cooling.

To improve the as-cast impact toughness of high chromium white irons, boron addition or use of rare earths is suggested aiming to refine the eutectic carbides; however, attempts to create such an effect through alloying do not find much success. Further, to improve wear performance of chromium white irons, it is quite common to hold the alloys at temperatures ranging between 900°C and 1100°C for 2 – 6h aiming to destabilize the metastable austenite. Destabilization at lower temperatures of 900°C and 950°C gives rise to excessive precipitation of secondary carbides, thereby producing carbon-depleted austenite susceptible to transform to low carbon martensite with poor wear resistance. In contrast, the higher destabilization temperature of 1000°C and above results in greater solubility of carbon in the austenite and subsequently limited precipitation of the secondary carbides. The carbon-rich austenite will then transform to harder martensite along with large content of retained austenite, expected to impair the matrix hardness and wear resistance. Post-destabilization tempering at subcritical temperatures followed by cryogenic holding below the martensite-finish ( $M_f$ ) temperature is expected to reduce the retained austenite content occurring with martensite. It is thought that a destabilized microstructure assuming optimum

combination of martensite, retained austenite and refined eutectic carbide can make a chromium white iron wear resistant and suitable for use in materials handling plants.

Keeping all the above-stated possibilities into consideration, the authors plan to undertake systematic studies on chromium white irons by developing three sets of alloy compositions bearing 8 wt.%, 16 wt.% and 20 wt.% chromium and then by conducting destabilization heat treatment of as-cast alloys. Before pursuing the said studies, a brief literature survey on high chromium white irons is endeavoured and presented as first chapter highlighting features on microstructure, hardness, impact toughness, wear resistance and electrochemical behaviour available in both as-cast and destabilized conditions. Thereafter, the second chapter includes sequentially the steps regarding preparation of the proposed alloys and evaluation of as-cast microstructures in terms of distribution of phases, development of hardness and wear behaviour. Third chapter describes the destabilization treatments performed and the experimental techniques utilized to assess the mechanical and wear properties developed. Subsequently, the fourth, fifth and sixth chapters present detailed analysis of destabilization treatments conducted in continuous as well as cyclic manner, evolving features for comparison with regard to microstructure, hardness, toughness, and wear resistance of the proposed alloys. In chapter seven, it is attempted to throw some light regarding electrochemical behaviour of the as-cast and destabilized alloys in saline solution with different pH levels; while in chapter eight, a summary is provided covering all the results. At last, chapter nine presents an elaborate (or general) discussion on all experimental findings, and also suggests for future scopes to carry out further studies.



# CHAPTER 1

## PUBLISHED WORKS ON CHROMIUM WHITE IRONS

DIPAK KUMAR MONDAL  
& SIDDHARTHA SANKAR MANDAL

### 1.1 As-cast High Chromium White Cast Iron

White cast irons are alloyed with chromium to produce high chromium white irons for applications requiring good abrasion resistance, toughness and corrosion resistance. This leads to the development of various commercial grade martensitic or austenitic white irons bearing 12 – 28 wt.% chromium. Considering iron, chromium, and carbon as the key elements present, high chromium white irons are classified as hypoeutectic, eutectic, and hypereutectic alloys<sup>1-3</sup>. The hypoeutectic compositions with 11 – 30% chromium and 2 – 2.8% carbon, give rise to as-cast microstructures possessing dendrites of primary austenite and thin inter-dendritic eutectic network of austenite plus carbide. Whereas, the hypereutectic Fe-Cr-C alloys containing >3% carbon, are supposed to contain massive primary  $M_7C_3$  carbides along with the eutectic of austenite plus  $M_7C_3$  carbide. In wear-resistant chromium white irons, chromium content below 12 wt.% also corresponds to the occurrence of continuous  $M_3C$  carbides with hardness of HV 1000 as well as duplex carbides possessing inner core of  $M_7C_3$  and outer shell of  $M_3C$ <sup>4,5</sup>. Chromium white irons requiring improved wear and fracture resistance suggest addition of chromium content beyond 12 wt.%, and this facilitates the formation of discontinuous and fibrous pattern of eutectic  $M_7C_3$  carbides bearing hardness up to HV1600.

#### 1.1.1 Composition

Chemical compositions of some common white iron alloys are given in Table 1.1, grouping them as Ni – Cr white irons (with low Cr and high C)

and high chromium white irons (with relatively low C) replacing costlier nickel by cheaper chromium. As is evident from this Table, manganese addition is quite common in both groups; while addition of reasonable content of molybdenum along with copper is practiced in high chromium white irons for reasons stated later in this section. Considering partial substitution of iron by chromium in Fe-Cr-C system, high chromium hypoeutectic alloys possess Cr/C ratios above 15 or more in comparison to the hypereutectic alloys with Cr/C ratios below 15.

Type	Elements, wt.%								
	C	Mn	Si	Ni	Cr	Mo	P	S	Cu
Ni-Cr-HC <sup>+</sup>	2.8-3.6	2.0	0.8	3.3-5.0	1.4-4.0	1.0	0.3	0.15	---
Ni-Cr-LC <sup>++</sup>	2.4-3.0	2.0	0.8	3.3-5.0	1.4-4.0	1.0	0.3	0.15	---
Ni-Cr-GB*	2.5-3.7	2.0	0.8	4.0	1.0-1.5	1.0	0.3	0.15	---
Ni-high Cr	2.5-3.6	2.0	2.0	4.5-7.0	7.0-11.0	1.5	0.1	0.15	---
12Cr	2.0-3.3	2.0	1.5	2.5	11.0-14.0	3.0	0.1	0.06	1.2
15Cr-Mo	2.0-3.3	2.0	1.5	2.5	14.0-18.0	3.0	0.1	0.06	1.2
20Cr-Mo	2.0-3.3	2.0	1.0-2.2	2.5	18.0-23.0	3.0	0.1	0.06	1.2
25Cr	2.3-3.3	2.0	1.5	2.5	23.0-30.0	3.0	0.1	0.06	1.2

Table 1.1 Chemical compositions of some common white iron alloys<sup>6</sup>

[Note: Single value represents maximum alloy content; \*GB- graphite bearing; <sup>+</sup>HC- high carbon; <sup>++</sup>LC- low carbon]

Although chromium content of commercial grade hypoeutectic alloys is quite high (between 10 and 30 wt.%), the majority of it is combined with carbon to form carbides. As a result, chromium content of the matrix is reduced largely arising poor hardenability for transformation of austenite to martensite on cooling. To overcome this issue, additional elements, namely, molybdenum, nickel, manganese, and copper are chosen for alloying with a view to achieve sufficient hardenability, particularly, with large castings. During alloying of chromium white irons, one should be careful with the problem of under-alloying responsible for austenite to pearlite transformation, and also with the risk of over-alloying that over-stabilizes the austenite phase. Anyway, the role of chromium and other elements, when added in white cast iron, is discussed below emphasizing the features appearing in connection with the eutectic pattern as well as the matrix microstructure.

**Chromium<sup>7</sup>:** Three major roles are played by chromium, when added in white cast irons. Primarily, it forms carbides; as a whole, it stabilizes the structure for high temperature applications, and precisely, it imparts corrosion resistance. The routinely added 2 – 3 wt.% chromium can ensure the formation of a graphite-free as-cast matrix in white cast iron containing

<1.0 wt.% silicon. Of course, such a low concentration of chromium has little or no effect on hardenability, because most of the chromium here is tied up to form  $M_3C$  eutectic carbides. Whereas greater chromium content of 10 – 20 wt.% changes the eutectic carbide from  $M_3C$  to  $M_7C_3$ , thereby making the hypoeutectic irons stronger and tougher<sup>8</sup>. Besides, chromium addition can be effective to develop resistance against softening as well as protection against oxidation during high temperature use. From oxidation point of view, 1.0 wt.% chromium is considered to be good enough for high temperature application up to 760°C; while 5.5 wt.% or more are required for temperatures beyond 760°C. For long term oxidation resistance at elevated temperatures, white irons with 15 – 30 wt.% chromium are preferred; although excessive chromium content can cause stabilization of the ferrite phase. The demand for wear-resistant, strong and tough white cast iron has led to the development of a series of martensitic and austenitic white irons containing 12 – 18 wt.% chromium. In all such cases of high chromium white irons, major part of chromium being converted to carbides, there is limited scope to suppress the eutectoid transformation of austenite to pearlite, or, in other words, to improve hardenability of the alloys. Hence, to obtain martensitic white irons, addition of molybdenum, nickel, manganese and copper becomes essentially required, and a detailed picture in this regard is placed as below.

**Molybdenum**<sup>9</sup>: Molybdenum addition is quite advantageous over other alloying elements for being typically effective to increase the depth of hardening, and so its addition is essentially carried out in heavy section components. Molybdenum is usually added in amounts between 1.0 and 3.0 wt.%, although its effectiveness to enhance the hardenability is better recognized by only 1.0 wt.% addition<sup>10</sup>. The hardenability improves further, when molybdenum is added in conjunction with nickel and copper<sup>11</sup>; however, the articles referred herewith do not cite any specific reason in support of this fact.

**Nickel**: When added in white cast iron, nickel is usually accommodated in the austenite or its transformation products. Simultaneously, it is a good graphitizer, and to counter this graphitizing effect of nickel, chromium is added in required proportions. When added in low-chromium white irons in amounts up to 2.5 wt.%, nickel produces finer pearlite structure, thereby introducing fair abrasion resistance. On the other hand, its addition up to 4.5 wt.% suppresses pearlite formation, and ensures production of wear-resistant martensitic white iron on normal cooling of the castings. Alternatively, to obtain wear-resistant martensitic large castings, addition of nickel up to 1.5 wt.% in conjunction with molybdenum is suggested;

otherwise, greater nickel content tends to stabilize the austenite phase. Besides, the amount of nickel is judiciously fixed along with the addition of chromium and copper to promote resistance to oxidation and scaling of chromium white irons at elevated temperatures.

**Copper:** In high chromium martensitic white irons, copper is added to suppress the transformation austenite to pearlite during post-solidification cooling, but never in excess of 1.2 wt.% to avoid retention of austenite with hardened martensite. It is suggested to add copper and molybdenum together in order to achieve required hardenability of the austenite in high chromium white irons.

### 1.1.2 Solidification Behaviour and Microstructure

Solidification of hypoeutectic alloys starts by the formation of primary austenite dendrites; while, the remaining liquid being rich in chromium and carbon later transforms to produce eutectic of austenite plus  $M_7C_3$  carbides, M representing the symbol for metallic species, iron and chromium. In hypereutectic alloys,  $M_7C_3$  carbides form first followed by solidification of the eutectic cells assuming alternate layers of  $M_7C_3$  carbide and austenite (martensite plus pearlite on transformation). Massive as well as rosetted morphology are quite common to identify  $M_7C_3$  primary carbides in alloys possessing higher chromium to carbon ratios. Whereas blade and rod shaped  $M_7C_3$  carbides appear with decreasing chromium to carbon ratios. Usually, alloy compositions producing primary  $M_7C_3$  carbides are avoided, except for use as short-blast blades, since primary  $M_7C_3$  are coarse to issue poor fracture resistance.

To obtain better insight regarding solidification of high chromium white irons, one can refer to the Fe-Cr-C liquidus surface, derived by Jackson<sup>12</sup> and subsequently revised by Thorpe and Chicco<sup>13</sup> to develop a microstructural map shown in Fig. 1.1. Evidently, majority of the white iron alloys of hypoeutectic variety, containing 12.0 – 30.0 wt.% chromium and 2.0 – 3.0 wt.% carbon solidify within the austenite field producing dendrites of primary austenite followed by eutectic cells made of austenite plus  $M_7C_3$ . During eutectic solidification, the available liquid momentarily reacts peritectically with  $M_7C_3$  to form  $M_3C$  walls around  $M_7C_3$  eutectic carbides, thereby stopping further reaction between  $M_7C_3$  and the remaining liquid. Fig. 1.1 also depicts that as the chromium content increases, carbon content of the eutectic decreases. When the chromium content falls below 10 wt.%, the eutectic reaction is altered involving production of  $M_3C$  eutectic carbide in place of  $M_7C_3$ .

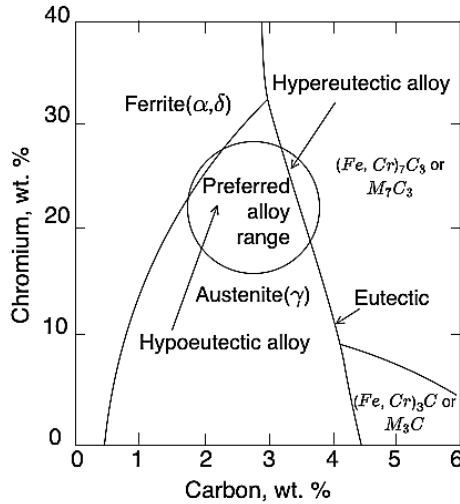


Fig. 1.1 Iron-chromium-carbon liquidus surface showing the composition range of commonly used hypoeutectic white irons<sup>14</sup>.

Although the austenite formed on solidification of hypoeutectic chromium white irons is likely to transform on cooling, a metastable austenite phase is still retained at ambient temperature subject to the condition that

1. the martensite start ( $M_s$ ) temperature is below the room temperature,
2. sufficient alloying elements are added to suppress the austenite to pearlite transformation on normal cooling, and
3. the rate of cooling is fast enough to avoid precipitation of secondary carbides in the austenite matrix.

It may be noted that, precipitation of secondary carbides reduces the alloy content of the surrounding austenite, and subsequently, raises its  $M_s$  temperature. Having the  $M_s$  temperature slightly above ambient temperature and the  $M_f$  below ambient, partial transformation of the matrix will issue martensite plus pearlite along with predominantly occurring austenite phase. Otherwise, the as-cast microstructure of hypoeutectic chromium white iron consists of austenite dendrites partially transformed to martensite, pearlite or bainite, and inter-dendritic eutectic of carbides and partially transformed austenite. Alloys closed to the eutectic composition usually do not possess the dendritic pattern of the matrix.

### 1.1.3 Eutectic Structure

Chromium being a strong carbide former, is considered to be a key element to produce eutectic carbides in white irons. Fig. 1.1 shows that as the chromium content of the alloy increases beyond 10 – 12 wt.%, the type of eutectic carbides changes from  $(\text{Fe, Cr})_3\text{C}$  to  $(\text{Fe, Cr})_7\text{C}_3$  following the rise in chromium to iron ratio and subsequent increase in hardness also. For years together, the structure of eutectic carbides was described as discontinuous pattern of rod and plate shaped particles. In early eighties, Powell<sup>5</sup> first undertook three-dimensional metallographic search to establish the continuous nature of eutectic carbides. Later, Laird<sup>15</sup> has specified the eutectic carbides as non-uniform mixture of randomly oriented rods with hexagonal cross section and hollow core filled with matrix material appearing around the carbides. Carbides of duplex nature<sup>4</sup> are also noticed to occur in Ni-Cr white irons and identified as  $\text{M}_7\text{C}_3$  encased with  $\text{M}_3\text{C}$ . Layers of  $\text{M}_3\text{C}$  around  $\text{M}_7\text{C}_3$  are believed to occur by solid state diffusion taking place during post-solidification cooling of the alloy following passage through  $\gamma + \text{M}_3\text{C}$  phase field in Fig. 1.1. Besides, occurrence of another variety<sup>16</sup> of duplex carbide, possessing stable  $\text{M}_{23}\text{C}_6$  shell around the metastable  $\text{M}_7\text{C}_3$  carbides, has been identified in white irons bearing 28 – 30 wt.% chromium and 2.0 – 2.7 wt.% carbon, when subjected to high temperature destabilization treatment.

Chromium white irons used for application requiring adequate toughness need to have refinement and, if possible, spheroidization of the eutectic carbides. This can be achieved by rapid cooling of the melt using chills during solidification, thereby enhancing nucleation rather than growth of the eutectic carbides. Alternatively, addition of boron (0.1 – 0.3 wt.%) in to the melt is suggested to refine the cast structure<sup>17</sup>. Whereas contradictory comments from researchers are unable to judge the effect of adding silicon and rare earths in modifying the carbide morphology. For example, when Shen and Zhou<sup>18</sup> have suggested extensive nucleation of eutectic carbides in white irons alloyed with high silicon, Laird and Powell<sup>19</sup> have commented just reverse. Similarly, Han and Wang<sup>20</sup> have identified rare earths as good carbide refining agents for Cr-Mn white irons; but Liang and Su<sup>21</sup> have reported no such beneficial role of rare earth addition towards refining eutectic carbides.

#### 1.1.4 Formation of $\text{M}_7\text{C}_3$ Carbides

Wear resistance of high chromium white irons attributes largely to the  $\text{M}_7\text{C}_3$ , which may form directly from the liquid as primary carbides, or may

precipitate as secondary carbides from the austenite with decreasing temperature. Occurrence of  $M_7C_3$  carbides directly from liquid in hypereutectic alloys provides sites for nucleation and growth of  $M_7C_3$  during eutectic reaction. Thus, a hypereutectic alloy consists of mainly  $M_7C_3$  carbides appearing as faceted hexagonal shaped particles, which can experience unrestricted growth among the rosette-type clusters formed by the eutectic reaction:  $Liquid \rightarrow M_7C_3 + austenite (\gamma)$ . In comparison to hypereutectic alloys, solidification of a hypoeutectic alloy involves prior formation of austenite ( $\gamma$ ) followed by a restricted growth of  $M_7C_3$  phase during eutectic reaction ( $Liquid \rightarrow M_7C_3 + \gamma$ ). In all cases, the carbide morphology is controlled by minimizing the interfacial free energy in a given volume of carbides and also the total elastic energy arising out of carbide-matrix as well as carbide-carbide interaction during nucleation and growth process<sup>22</sup>. In addition, the local constraints associated with the growth process happen to affect the carbide shape and size<sup>23, 24</sup>.

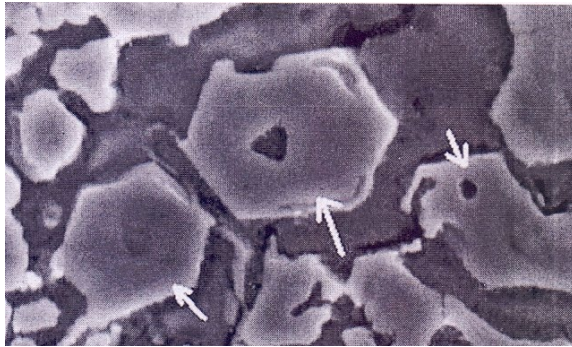


Figure 1.2 SEM showing hexagonal shell(arrow) of  $M_7C_3$  carbide in dark matrix of austenite<sup>8</sup> (5000X).

As shown in Fig. 1.2, the chromium-rich  $M_7C_3$  carbides occur as hexagonal shells growing inwardly with shrinking cavities at the central zone. Liquid remaining in a central cavity solidifies to form austenite, which being deficient with carbon and chromium content later transforms to martensite on cooling. Steps associated with forming such hexagonal morphology of  $M_7C_3$  carbides are described below along with illustrations displayed in Fig. 1.3a - f:

Step 1. Nucleation of austenite along with growing austenite (A) islands in an undercooled liquid/melt (Fig. 1.3a).

Step 2. Growth of austenite nuclei with rejection of carbon and chromium and their subsequent build-up around the growing austenite island (Fig. 1.3*b*).

Step 3. Nucleation of  $M_7C_3$  carbides at the austenite periphery following diffusion of carbon and chromium atoms from the surrounding liquid to  $M_7C_3$  nuclei (Fig. 1.3*c*).

Step 4. Growth of  $M_7C_3$  carbides by more and more carbon and chromium atoms leaving the liquid and joining the carbide particles (Fig. 1.3*d*).

Step 5. Formation of austenite nuclei and their growth in the carbon and chromium depleted liquid adjacent to  $M_7C_3$  (Fig. 1.3*e*), and subsequent recurrence of steps 2 – 4.

Step 6. Formation of secondary carbides at  $M_7C_3$  and/or within austenite (martensite on transformation) following decrease in the solubility of carbon and chromium in austenite during solid-state cooling (Fig. 1.3*f*). Growth of these secondary carbides leads to connectivity between the adjacent  $M_7C_3$  carbides.

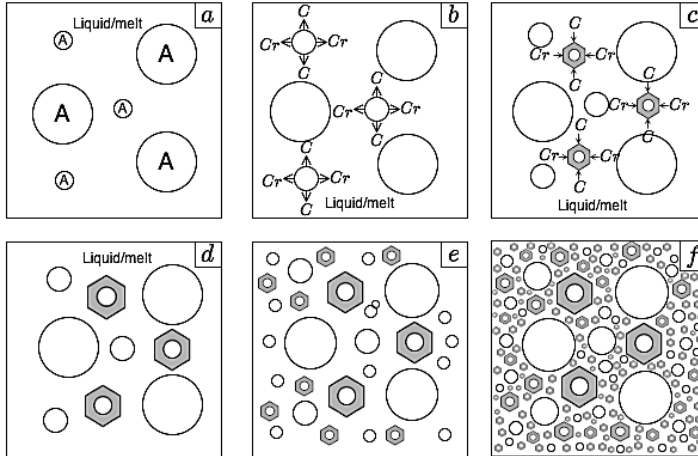


Fig. 1.3 Steps illustrating formation of austenite (A) and hexagonal morphology of  $M_7C_3$  carbides.

Following steps 2 – 4 in the first round as well as step 5 in the second round, nucleation and subsequent growth of  $M_7C_3$  carbides can produce pencil-like structure in a rosetted cluster, as shown in Fig. 1.4. Similar steps of nucleation,